COBEM 99
XV Congresso Brasileiro de Engenharia Mecânica
15th Brazilian Congress of Mechanical Engineering
22 - 26 de Novembro de 1999 / November 22 - 26, 1999 Águas de Lindóia, São Paulo,

PERFORMANCE OF LOW-REYNOLDS κ-ε MODELS TO PREDICT FLOW THROUGH CURVILINEAR OBSTRUCTION

G. N. Zevallos
gzevallo@mec.puc-rio.br
A. O. Nieckele
Departamento de Engenharia Mecânica, Pontifícia Universidade Católica – PUC/Rio
R. Marquês de São Vicente 225- Gávea, 22453-900 Rio de Janeiro, RJ, Brasil
nieckele@mec.puc-rio.br

Abstract. *At the present work the performance of three different low Reynolds number κ–ε turbulence models, for the prediction of flows in the presence of separation and reattachment, is investigated. The geometry of interest consist of a duct with curvilinear obstruction described by a cosine curve. The objective of the analysis is to verify if the models selected are capable of capturing the recirculation areas and pressure recovery after the obstruction, fundamentals for the evaluation of the distribution of tensions. The fields of velocity, turbulent kinetic energy and dissipation rate were obtained by the different models. Comparison with numeric and experimental data found in the literature is performed, seeking to identify which model is more adapted for those type of flows. The numeric determination of the fluid flows was accomplished by a finite volume method with non-orthogonal curvilinear coordinates, which adapts to the geometry. The countervariants velocity components were employed as independent variables in the momentum conservation equation and the velocity-pressure coupling was solved by the SIMPLEC algorithm. Among all tested models, none was able to reproduce exactly the experimental data. Satisfactory mean velocity and pressure distribution were obtained, however, poor results were encountered for the turbulent quantities.*

Key-words: *low Reynolds κ-ε models, Curvilinear obstruction*

1. INTRODUCTION

Flow field in curvilinear obstructions is often found in engineering as well as biomedical applications. An example that can be mentioned is the presence of weld joints in small diameter ducts which causes localized corrosion after the restriction. In general, for engineering situations, the flow is in the turbulent regime. The prediction of the pressure recovery and the shear distribution along the obstruction can help to design equipment to avoid the corrosion. In the biomedical area, arteries obstruction is a mayor problems for the circulatory system (Rastogi, 1984).

Numerical simulation of flow field has become an excellent tool to help develop projects and process that are more efficient at a lower cost. For engineering applications, in general the

flow field is turbulent. Since turbulent flow is three dimensional and transient, the computing effort to obtain directly the velocity and pressure field, especially in complex geometries, is very high. An attractive alternative from the practical point of view is to employ turbulence models to predict the time average variables of interest. Among the two equation differential models available, the high Reynolds numbers κ–ε model is still the model more widely used to solve practical engineering problems. The traditional κ-ε model has been significantly enhanced to be applied to the whole domain, i.e, in the near wall region as well as in the turbulent core. These models are called low Reynolds number κ-ε models (LRN), since they can predict the flow behavior near the walls, where the Reynolds number is low. Along the last decades, several works have been published, with different variants of the model. Just a few of them are referred here: Jones and Launder, 1972, Patel and Rodi, (1985), Koobus (1994), Geronimos and So (1997) and Chen et al. (1998).

The main objective of the present work is to analyze the performance of different low Reynolds number κ–ε models to predict the flow field in ducts with obstruction. After a vast literature survey, three models were selected to be presented here. The models selected were developed by Hanjalic and Launder (1980), Abe, Kondoh and Nagano (1994) and Sarkar e So (1997).

2. ANALYSIS

The geometry selected to be analyzed at the present work consists of a duct with circular cross-section, with a curvilinear obstruction as illustrated in Fig. 1. The obstruction is defined by a stenosis type of curve, described by the following expression

$$\frac{R_C}{R_O} = 1 - \frac{\delta}{2R_O}\left(1 + \cos\frac{\pi x}{x_O}\right) \tag{1}$$

where R_c is the duct radius, R_o the unobstructed duct radius, δ is restriction height, x is the axial coordinate and x_o is the restriction half length. The dimensionless parameters that characterized the obstruction were set as $x_o/R_o = 2$ and $\delta/R_o = 0.5$. This configuration was experimentally investigated by Deshpande e Giddens, 1980. Numerical investigation based on the standard κ–ε model has also been performed for this configuration by Rastogi (1984), Melaaen (1992) e Zijlema et al. (1995). The length of the straight duct upstream and downstream the obstruction were set at $x_{up}/R_o = 2$, and $x_{dn}/R_o = 14$.

To obtain the flow field in a horizontal axi-symmetric duct, the following hypotheses were made: Newtonian fluid, constant properties and steady state regime. The average continuity and momentum equations, can be written as:

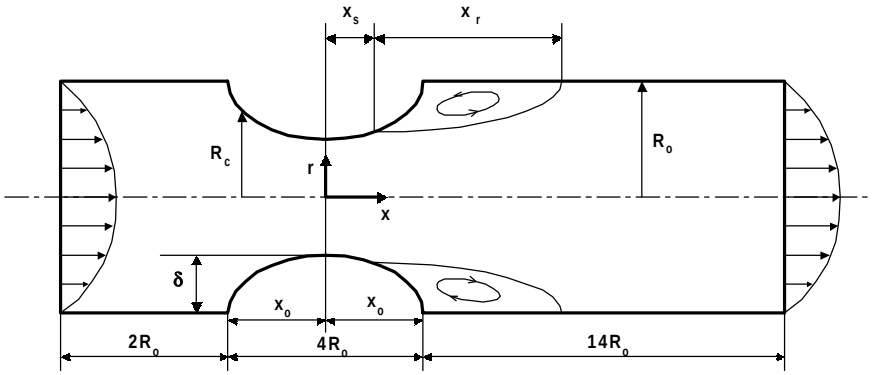

Figure 1- Duct with curvilinear obstruction.

$$\frac{\partial u_i}{\partial x_j} = 0 \tag{2}$$

$$\rho u_j \frac{\partial u_i}{\partial x_j} = \frac{\partial}{\partial x_j}\left[(\mu + \mu_t)\left(\frac{\partial u_i}{\partial x_j} + \frac{\partial u_j}{\partial x_i}\right)\right] - \frac{\partial P}{\partial x_i} \tag{3}$$

where u_j are the velocity components, x_j the coordinate directions, μ and μ_t are the absolute and turbulent viscosity, ρ is the density and P is a modified pressure [$P = p + (2/3)\,\rho\,\kappa$], where κ is the turbulent kinetic energy.

After an extensive search through the specialized literature, three models were selected based on their ability to represent the flow near the wall. The models selected are SSA, developed by Sarkar e So, (1997), NT of Abe, Kondoh and Nagano (1994) and LSH developed by Launder and Sharma and modified by Hanjalic, (Hanjalic and Launder, 1980). The κ–ε conservation equation for the three models can be represented by the following equations, where $\hat{\varepsilon}$ is a modified dissipation rate of κ.

$$\rho\, u_j \frac{\partial\, \kappa}{\partial\, x_j} = \frac{\partial}{\partial\, x_j}\left[\left(\mu + \frac{\mu_t}{\sigma_\kappa}\right)\frac{\partial\, \kappa}{\partial\, x_j}\right] + P_\kappa - \rho\, \hat{\varepsilon} + L_\kappa \tag{4}$$

$$\rho\, u_j \frac{\partial\, \hat{\varepsilon}}{\partial\, x_j} = \frac{\partial}{\partial\, x_j}\left[\left(\mu + \frac{\mu_t}{\sigma_\varepsilon}\right)\frac{\partial\, \hat{\varepsilon}}{\partial\, x_j}\right] + C_{\varepsilon 1} P_\kappa \frac{\hat{\varepsilon}}{\kappa} - C_{\varepsilon 2}\, f_2\, \rho\, \frac{\hat{\varepsilon}^2}{\kappa} + L_\varepsilon \tag{5}$$

In the above equation, the turbulent viscosity is

$$\mu_t = f_\mu\, c_\mu\, \rho\, \frac{\kappa^2}{\hat{\varepsilon}} \tag{6}$$

and P_κ is the production of turbulent kinetic energy, given by

$$P_\kappa = \mu_t \left[\frac{\partial u_i}{\partial x_j} + \frac{\partial u_j}{\partial x_i}\right]\frac{\partial u_i}{\partial x_j} \tag{7}$$

The main differences among the models are the damping functions to represent the flow near the walls and additional low Reynolds source terms in the κ and ε conservation equations. Further, while SSA and NT solve for $\hat{\varepsilon} = \varepsilon$, the LSH model solves for $\hat{\varepsilon} = \tilde{\varepsilon}$, a pseudo dissipation rate of the turbulent kinetic energy $\tilde{\varepsilon}$ defined as $\varepsilon - \varepsilon^*$, where

$$\varepsilon^* = 2\frac{\mu}{\rho}\left(\frac{\partial\sqrt{\kappa}}{\partial x_j}\right)\left(\frac{\partial\sqrt{\kappa}}{\partial x_j}\right) \tag{8}$$

Consequently different boundary condition for $\hat{\varepsilon}$ must be given. It is zero por LSH model, and ε^*_{wall} for the two others models. The NM model simplifies the expression to $\varepsilon^*_{wall} = 2\,\mu\,/\,\rho\,(\partial\sqrt{\kappa}\,/\,\partial\, n)^2 \approx 2\mu\,\kappa\,/(\rho\, n^2)$, which is easier to evaluate. Table 1 summarizes the differences among the models.

Tabela 1. κ–ε source and damping functions

	SSA	NT	LSH
L_κ	0	0	$\rho\varepsilon$ *
L_ε	$exp[-(Re_t/40)^2]$ $[-0.57\rho\varepsilon\tilde{\varepsilon}/\kappa +$ $+0.5\rho(\varepsilon_{wall}^*)^2/\kappa -$ $2.25P_\kappa\varepsilon/\kappa]$	0	$(C_{\varepsilon 3} - C_{\varepsilon 1})\ P_\kappa^* \left(\frac{\tilde{\varepsilon}}{\kappa}\right) -$ $\frac{2\mu\mu_t}{\rho}\left[\frac{\partial}{\partial x_j}\left(\frac{\partial u_i}{\partial x_k}\right)\right]^2$
f_μ	$(1+3/Re_t^{3/4})$ $[1+80exp(-Re_\varepsilon)]$ $[1-exp(-Re_\varepsilon/43-Re_\varepsilon^2/330)]^2$	$[1-exp(-Re_\varepsilon/14)]^2$ $[1+(5/Re_t^{3/4})\ \{-(Re_t/200)^2\}]$	$exp[-3.4/(1+0.02Re_t)^2]$
f_2	$\tilde{\varepsilon}\ /\ \hat{\varepsilon}$	$[1-exp(-Re_\varepsilon/3.1)]^2$ $[1-0.3exp\{-(Re_t/6.5)^2\}]$	$1-0{,}3\ exp(-Re_t^2)$

The empirical constants are also slightly different for each model. For the SSA model, they are: $C_\mu = 0.096$; $\sigma_\kappa = 1.0$; $\sigma_\varepsilon = 1.45$; $C_{\varepsilon 1} = 1.05$; $C_{\varepsilon 2} = 1.83$; $C_{\varepsilon 3} = 0.0$. For the NT model: $C_\mu = 0.090$; $\sigma_\kappa = 1.4$; $\sigma_\varepsilon = 1.40$; $C_{\varepsilon 1} = 1.50$; $C_{\varepsilon 2} = 1.90$; $C_{\varepsilon 3} = 0.0$. And for the LSH model: $C_\mu = 0.090$; $\sigma_\kappa = 1.0$; $\sigma_\varepsilon = 1.30$; $C_{\varepsilon 1} = 1.44$; $C_{\varepsilon 2} = 1.92$; $C_{\varepsilon 3} = 0.44$.

P_κ* corresponds to the contribution to the production of κ due to only the normal shear stresses. The damping functions are dependent on the following local Reynolds number, related to local variables and the wall distance *n*.

$$Re_t = \frac{\rho\,\kappa^2}{\mu\,\hat{\varepsilon}} \qquad ; \qquad Re_\varepsilon = \frac{(\mu\ \varepsilon\ /\ \rho)^{1/4}\ \rho\ \varepsilon\ n}{\mu} \tag{9}$$

2.1 Boundary conditions

At the inlet, a fully developed velocity profile, u_{in}, was specified in accordance with the experimental data of Deshpande and Giddens 1980, as

$$u_{in} = 1.25\,u_m\,\left(1\ -\ r/R_o\right)^{1/6.4} \tag{10}$$

where u_m is the mean velocity at the cross section. The boundary condition for the turbulent quantity κ was specified as $\kappa_{in} = 1.5\ I_{it}^2\ u_{in}^2\ /\ 2$, where I_{it} is the turbulence intensity, defined as 3% in accordance with Melaaen (1992) and Zijlema et al, (1995). For the dissipation rate, based on the recommendation of Shinha e Candler, (1998), the following expression was adopted, $\varepsilon_{in}=c_\mu^{3/4}\kappa_{in}^{3/2}/(4\ \ell_{in})$, with $\ell = \min[\ K\ (R_O - r);\ 0.1\ R_O\ ]$, where ℓ is the mixing length is and $K=0.4$ is the von Kármán constant.

At the symmetry line, the normal velocity component was set equal to zero as well as the normal gradient of all others variables. At the exit plane, the traditional boundary condition of neglecting the diffusion flux of all variables was employed. At the solid surfaces, the non-slip condition was enforced.

3. NUMERICAL METHOD

A non-orthogonal curvilinear system of coordinates, which adapts to the boundaries of the domain, was employed. This is an important technique, which allows an easy and exact representation of the boundary conditions, making it possible to solve turbulent flow field in complex geometries. The conservation equations are discretized with the aid of the finite volume method described in Patankar (1980), using the *power-law* scheme. Staggered velocity components were used to avoid unrealistic pressure fields, and the contra-variant velocity component was selected as the dependent variable in the momentum conservation equations (Pires and Nieckele, 1994). The pressure-velocity coupling was solved by an algorithm based on SIMPLEC (van Doormaal and Raithby, 1984). The resulting algebraic system was solved via the TDMA line-by-line algorithm (Patankar, 1980) with the block correction algorithm (Settari and Aziz, 1973) to increase the convergence rate.

To define the mesh size a grid test was performed, where different mesh sizes and distribution were investigated. Finally, a non-uniform 115 x 60 points mesh was specified to analyze the numerical prediction of the three turbulence models. The grid points were concentrated near the solid wall and the obstruction region. The mesh was generated by the commercial software FLUENT (FLUENT, Inc.V 4.4, 1996).

4. RESULTS

The present problem is governed by the several geometric parameters presented and by the Reynolds number defined as $Re = \rho\ u_m\ 2\ R_o\ /\ \mu$. For the present work, the Reynolds number was set equal to 15 000.

To evaluate the turbulence models selected, the velocity, pressure and turbulence quantities fields were compared with experimental data of Desphande and Giddens (1980), and the numerical results of Rastogi (1984) and Melaaen (1992), both based on the traditional κ–ε model.

Rastogi (1984) solution was obtained with a 41 x 21 mesh with an orthogonal coordinate system. It was based on the hybrid scheme, with the covariant velocity components as the dependent variable in the momentum equations. Melaaen (1992) solution was obtained with a non-orthogonal coordinate system, with colocated cartesian velocity as the dependent variable, with a mesh size of 52 x 22 nodal points. Melaaen (1992) investigated two interpolation schemes. The first one, based on the power-law scheme, is not presented here, because the results obtained were slightly worse than the ones obtained by Rastogi (1984) with an equivalent interpolation scheme. The second case, selected to be compared here, employed a second order upwind interpolation scheme for the velocities and the power-law scheme for the turbulent quantities. The same geometry was also investigated with the traditional κ–ε model by Zijlema et al, (1995). However, very poor results were obtained and their results will not be presented here.

4.1 Pressure and velocity distribution

To analyze the pressure prediction along the wall, a pressure coefficient was defined based on the inlet pressure p_{in} and mean velocity u_m as

$$C_p = \frac{p - p_{in}}{\rho\ u_m^2} \tag{11}$$

The pressure distribution along the pipe wall is presented at Fig. 2. It can be seen that all schemes present a similar behavior in the upstream and convergent section of the duct. All

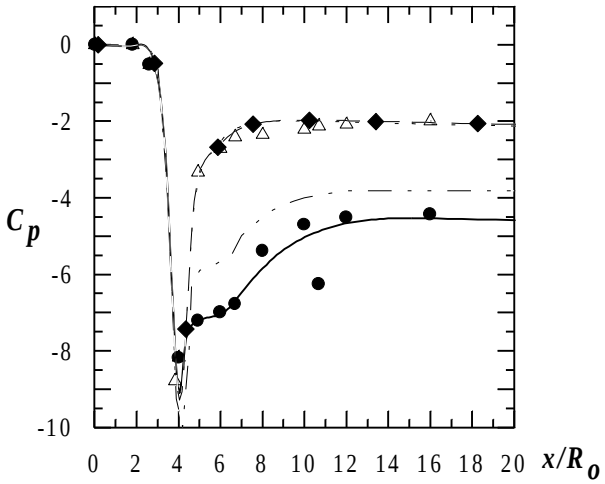

Figure 2 – Pressure coefficient

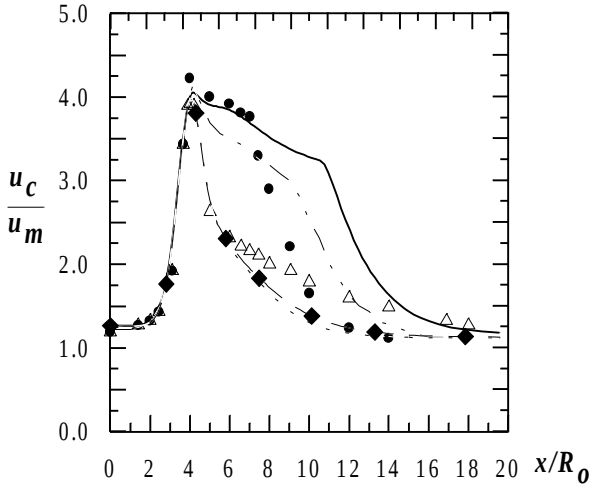

Figure 3 – Centerline velocity distribution

legend : NT model SSA model LSH model
Rastogi (1984) Melaaen (1992) Desphande & Giddens (1980)

schemes super-estimate the minimum pressure, which occurs at the center of the obstruction (x/R_o = 4). At the divergent section and at the downstream portion of the duct through the exit (4 < x/R_o < 20), only the LHS model is able to satisfactory reproduce the smooth pressure recovery, presenting good agreement with experimental data. The SSA and NT models cannot capture this behavior. Their predictions are equivalent and similar to the results obtained by Rastogi (1984) with the traditional κ–ε model. Pressure is super-estimate after the obstruction. The pressure distribution obtained with the higher order scheme of Melaaen (1992), with the traditional κ–ε model, is similar to the results of LSH, however the pressure after the obstruction is still higher than the experimental data.

Figure 3 illustrates the dimensionless centerline velocity distribution. Again, the same behavior is observed for all models at the convergent section, and the maximum velocity is under estimated by all models. It is 6% lower for the SSA and NT low Reynolds κ–ε models, as well as for the traditional κ–ε models and 4% lower for the LSH model. Although the LSH underestimates the maximum velocity, it is capable of capturing the flow desacceleration at the divergent region, up to the section x/R_o = 6, since an excellent agreement with the experimental data is observed. After the end of the obstruction, x/R_o = 8, it can be seen from the experimental data, a fast velocity recovery to its initial value at x/R_o = 14. The LSH model does not predict this desacceleration. It is only at x/R_o = 10.5 that a strong desaccelaration is observed. The SSA and NT models present equivalent results with a strong desacceleration immediately after the end of the obstruction, and a slower velocity recovery than the other methods. The higher order method presents a velocity distribution analogous to the LSH model, however its velocity recovery is premature.

Figure 4 illustrates the streamlines obtained with the three low Reynolds number κ–ε models, where a recirculation region can be easily seen. The same levels were selected for all cases. The isolines were uniformly distributed inside and outside the recirculation region. LSH model predicts a much larger recirculation region than other models, with its center located near the end of the obstruction (x/R_o = 6). Again, the results obtained with the SSA and NT models are equivalent.

4.2 Friction factor and reattachment point

Although the streamline distribution allows us to identify the recirculation region, the friction factor distribution along the wall helps us to precisely determine its size.

(a) NT model

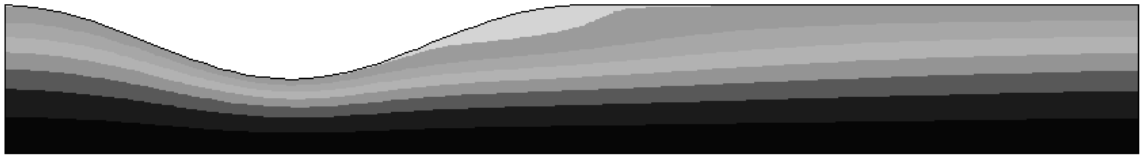

(b) SSA model

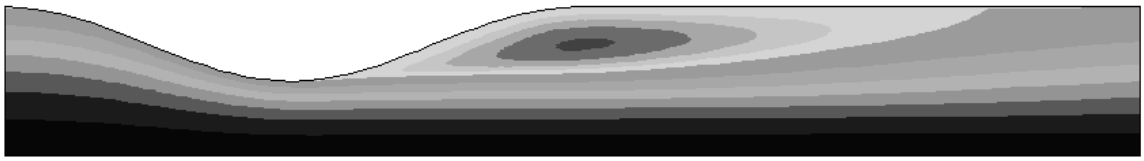

(c) LSH model

Figure 4 – Streamline distribution

The friction factor, or dimensionless wall shear stress, τ_s, can be defined as

$$C_f = \frac{\tau_s}{0.5\ \rho\ u_m^2} \tag{12}$$

The friction factor distribution along the wall is shown in Figure 5 for the three models selected. These values were not available for the traditional κ–ε model, and they will not be presented here. It can be seen in Fig. 5, that the shear stress increases at the convergent region of the duct, reaching a maximum value at the center of the obstruction, with a very sharp drop right after it. The separation point is clearly identified as the position where the shear stress is zero. After this point, the shear stress becomes negative indicating the recirculation region. As already seen by the streamlines distribution, NT and SSA models, present a small recirculation region, with a reattachment point approximately equal to $6\ R_o$. As the others models, LSH model presents an increase of the shear stress after the separation point. However, near the end of the obstruction region, close to the center of the recirculation, where the reverse flow is stronger, a decrease in the shear stress is observed. After which, the shear increases again. Consequently, the reattachment point is moved downstream ($x/R_o \approx 9$).

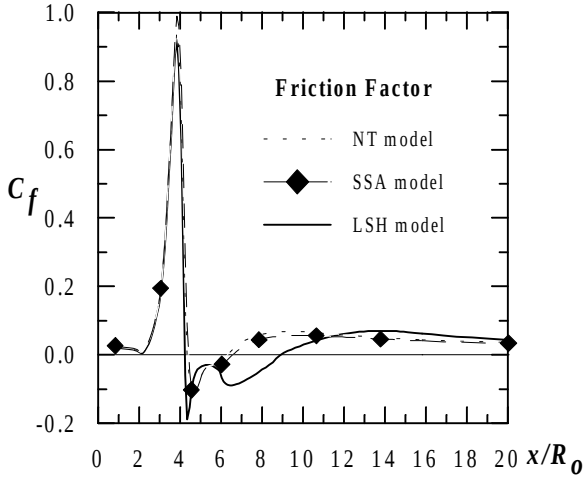

Figure 5 –Friction factor

Table 2 – Separation and reattachment points

Model	Mesh	x_{dn}/R_o	x_s/R_o	x_r/R_o
Desphande e Giddens, 1980 (experimental)			≈4,4-4,5	8,0
Rastogi, 1980	41 x 21	11	5,2	6,4
Melaaen, 1992	52 x 22	12	4,56	8,07
NT	110 x 60	14	4,35	6,33
NT	57 x 22	14	4,64	6,79
SSA	110 x 60	14	4,41	6,65
SSA	57 x 22	14	4,65	7,60
LSH	110 x 60	14	4,23	8,92
LSH	57 x 22	14	4,63	7,81

Table 2 presents a comparison of the separation and reattachment points, x_s and x_r,, predicted by the three low Reynolds number κ–ε models and the results of Rastogi (1984) and Melaane (1992) obtained with the traditional κ–ε models. The experimental results of Desphane and Giddens (1980) are also shown at the table. Since different mesh sizes were employed by each author, this information is also presented at Table 2. The downstream length, x_{dn}, was not informed at the experimental work, but it is known that this is a critical parameter for the numerical simulation because of the zero diffusion flux boundary condition employed, so this information is also provided at Table 2.

By examining Table 2, it can be seen that the higher order scheme with the traditional κ–ε model (Melaaen, 1992) presented the best agreement with experimental data, for both separation and reattachment points. Since the number of grid points employed by Melaaen (1992) was smaller, the low Reynolds κ–ε models were also solved with a smaller mesh size, equivalent to the Melaaen's work. It can be seen that greater discrepancies with the experimental data is obtained with the NT and SSA models when the mesh size is made smaller. The LSH model under predicts the separation and reattachment points for the course mesh and over predicts it for the fine mesh. The worse result was predicted by Rastogi (1984), however, they are not very different than the ones predicted by the NT and SSA models.

4.3 Turbulence quantities

The only turbulence quantity available in the literature to allow a comparison with the present results is the turbulent kinetic energy. Figure 6 present its dimensionless distribution, κ/u_m^2, along the centerline. It can be seen that the agreement of the different numerical and turbulent models with experimental data is not satisfactory. The experimental data show an approximately constant κ up to the section of maximum obstruction. Along the region where pressure is recovered, there is a substantial increase of κ, followed by a strong decrease. The resulting profile is almost symmetric. The section where κ starts to fall corresponds to the section where pressure has reached its downstream level, as can be seen in Fig. 2.

All models presented a sharp increase of κ along the centerline followed by its reduction, however, the section where the maximum occurs, as well as the maximum value are quite different for each case. Note that the maximum κ always corresponds to the point where pressure has reach a constant value. This behavior can also be observed by the experimental data. Rastogi (1980) presents the greater discrepancies with the experimental data. Melaaen (1992) results have two picks of κ. The first one over estimates κ, while the second one is quite close to the experimental data, as well as to the LSH model results. The LSH model is not able to reproduce the increase in κ at the obstruction region. It presents a sharp increase of κ, right after the reattachment point. To understand the results obtained, isocurves of turbulent

kinetic energy are presented at Fig. 7 for the three low Reynolds number κ–ε models. The same isolines uniformly spaced were selected. Again, the predictions of the NT and SSA models are similar. Low κ values are seen by the dark color near the entrance. The turbulent kinetic energy begins increases at the obstruction, as one can see the colors getting lighter. Then it reaches a maximum value at the recirculation region, when a new dark color appears. The kinetic energy is generated near the wall and then it is convected throughout the domain. The recirculation region predicted by the LSH model is much larger than the other models, and its center of rotation is displaced downstream, as a consequence the maximum turbulent kinetic energy generation also occurs displaced to downstream. The high value generated are then convected, and the increase in κ at the centerline is only seen at section x/R_o = 12.

5. Conclusion

At the present work the ability of three low Reynolds number κ–ε models to predict turbulent flow in duct with smooth obstruction was examined. It was verified that although

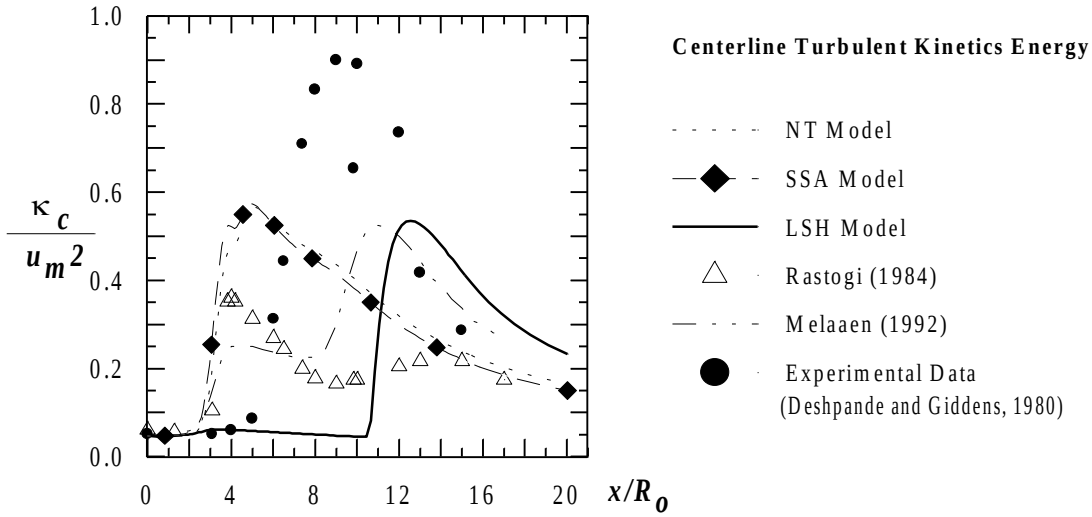

Figure 6 – Centerline turbulent kinetic energy distribution

(a) NT model

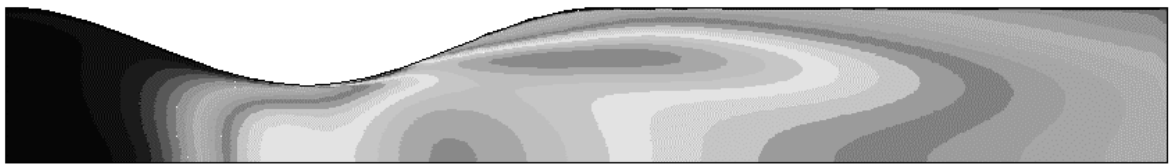

(b) SSA model

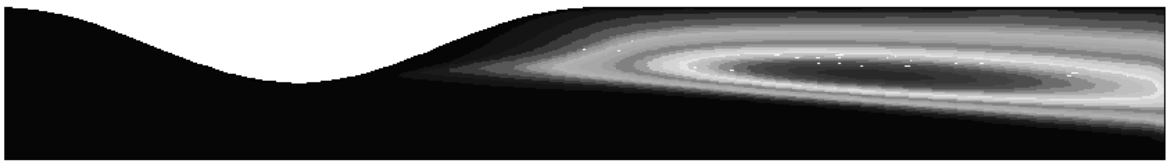

(c) LSH model

Figure 7 – Turbulent kinetic energy distribution

the velocity and pressure distributions were reasonable predicted by the different models, all of them fail to predict correctly the turbulent quantities. The LSH model presented the best agreement with experimental data. However, the higher order interpolation scheme with the traditional κ–ε model, also predicted good results. The SSA and NT models are not adequate to predict separation along smooth surfaces, because the low Reynolds models are more expensive and harder to converge and these models presented results equivalent to cheaper and easier to implement traditional κ–ε models. It seems that a combination of a higher order scheme and the LSH model should be investigated.

REFERENCES

Abe K., Kondoh T., Nagano Y., 1994, A New Turbulence Model for Predicting Fluid Flow and Heat Transfer in Separting and Reattaching Flows Part: I Flow Field Calculation, Int. Journal Heat and Fluid Flow, vol 18, n.^{o} 3, pp 266,282.

Chen S., Lai J., Milthorpe, J., Mudford N., 1998, A New Modified Low-Reynolds Number κ–ε Model, 29th AIAA Fluid Dynamic Conference, AIAA 98-2553.

Desphande M. D., Giddens D.P. 1980, Turbulence Measurement in a Constricted Tube, Journal Fluids Mechanics, vol 97, pp 65-89, Part 1.

Geronimos G., So R. M.C., 1997, Near-Wall Modeling of Plane Turbulent Wall Jets, J. of Fluids Engineering, vol 119, pp 304-313, June, 1997.

Hanjalic K, Launder B.E., 1980, Sensitizing the Dissipation Equation to Irrotational Strain, Journal of Fluids Engineering, vol 102, pp 34-40, March, 1980.

Jones W.P., Launder B.E., 1972, The Prediction of the Laminarization with a two-equation model of turbulence, International Journal Heat Mass Transfer, vol. 15: 301-314.

Koobus B., 1994, An Implicit Method for Turbulent Boundary Layers Simulation, Programme 6 –Calcul scientifique, modélisation et logiciel numérique, , Unité de Recherche INRIA Sophia - Antiopolis, Décembre 1994, 38 pages.

Melaaen M. C., 1992, Analysis of Fluid Flow in Constricted Tubes and Ducts Using Body-Fitted Non-Stagered Grids, Intenational Journal for Numérical Methods in Fluids, vol 15, pp 895-923.

Patankar S. V. , 1980, Numerical Heat Transfer and Fluid Flow, Hemisfere, New York.

Patel V., Rodi W., Scheuerer G., 1995, Turbulence Models for Near-Wall and Low-Reynolds Number Flows: A Review, AIAA Journal, vol 23, N^{o}9, pp1308-1319.

Pires, L. F. G. and Nieckele, A. O., 1994, Numerical Method For The Solution Of Flows Using Contravariant Components In Non-Orthogonal Coordinates, Proc. V Brazilian Meeting on Thermal Sciences, SP, pp. 343-346 (in Portuguese).

Rastogi A. K., 1984, Hydrodinamics in Tubes Perturbed by Curvilinear Obstructions, Journal of Fluids Enginnering, vol 106, pp 262-269, September 1984.

Sarkar A., So R.M., 1997, A Critical Evaluation of Near Wall Two-Equations Models Against Direct Numerical Simulation Data, Int. J. Heat and Fluid Flow, vol 18, pp 197-208.

Settari A., Aziz K., 1973, A Generalizarion of the Additive Corrections Methods for the Iterative Solution of Matrix Equations, SIAM, J.Num Analysis, vol. 10, pp. 506-521.

Sinha K., Candler G.**,** 1998, Convergence Improvement of Two-Equation Turbulence Models Calculations, 29 th AIAA Fluid Dynamics Conference, AIAA 98-2649.

Van Doormaal, J. P. Raithby, G. D., 1984, Enhancements of the Simple Methods for Prediction Incompressible Fluid Flow, Num. Heat Transfer, vol 7, pp147-163.

Zijlema M., Segal A., Wessling P., 1995, Finite Volume computation of 2D incompressible turbulent flows in general coordinates on staggered grids, March 10th, 1998, http: //www.dutita0.twi .tudelft .nl/isnas/report94-24/isrep2.html.